Migratory Transmetalation in Diphenoxo-Bridged $Cu^{II}M^{II}$ Complexes of a Dinucleating Macrocycle with $N(amine)_2O_2$ and $N(imine)_2O_2$ Metal-Binding Sites

Masami Yonemura, Yukiko Matsumura, Hideki Furutachi, Masaaki Ohba, and Hisashi Ōkawa*

Department of Chemistry, Faculty of Science, Kyushu University, Hakozaki, Higashiku, Fukuoka 812, Japan

David E. Fenton

Department of Chemistry, The University of Sheffield, Sheffield S3 7HF, U.K.

Received December 4, 1996[⊗]

A phenol-based heterodinucleating macrocycle (H_2L), comprised of two 2-((methylamino)methyl)-6-(iminomethyl)-4-bromophenolate entities bridged by the $-(CH_2)_2-$ groups between amine nitrogens and by the $-(CH_2)_3-$ groups between imine nitrogens, displays dissimilar $N(amine)_2O_2$ and $N(imine)_2O_2$ metal-binding sites sharing the phenolic oxygens and is prepared as a Cu(II)Pb(II) complex $[CuPb(L)](ClO_4)_2$. An analogous complex $[CuPb(L)(BzO)(dmf)]ClO_4$ crystallizes in the triclinic space group $P\bar{1}$, (No. 2), with $a = 13.998(2)$ Å, $b = 15.568(2)$ Å, $c = 8.699(2)$ Å, $\alpha = 95.32(1)°$, $\beta = 92.23(1)°$, $\gamma = 82.81(1)°$, $V = 1871.9(5)$ Å^3, and $Z = 2$. Refinements based on 3788 reflections with $I > 3.00\sigma(I)$ converged with $R = 0.058$ and $R_w = 0.069$. The Cu(II) resides at the $N(imine)_2O_2$ site and assumes a planar geometry. The Pb(II) resides at the $N(amine)_2O_2$ site and assumes a seven-coordinate geometry by further addition of a dmf molecule and a bidentate benzoate group. The Cu--Pb separation, doubly bridged by the phenolic oxygens, is 3.466(2) Å. The reaction of $[CuPb(L)](ClO_4)_2$ with metal(II) sulfate salts provides $Cu^{II}M^{II}$ complexes $[CuM(L)](ClO_4)_2 \cdot nH_2O$ (M = Mn ($n = 2$), Co ($n = 2$), Ni ($n = 0$), Cu ($n = 0$), Zn ($n = 1$)). The CuZn complex, $[CuZn(L)(AcO)]ClO_4$, crystallizes in the triclinic space group $P\bar{1}$, (No. 2), with $a = 12.290(3)$ Å, $b = 13.402(4)$ Å, $c = 11.501(2)$ Å, $\alpha = 95.10(2)°$, $\beta = 116.68(2)°$, $\gamma = 112.00(2)°$, $V = 1491.8(9)$ Å^3, and $Z = 2$. Refinements based on 2497 reflections with $I > 3.00\sigma(I)$ converge with $R = 0.046$ and $R_w = 0.034$. The Cu(II) is bound at the $N(amine)_2O_2$ site and the Zn(II) is bound at the $N(imine)_2O_2$ site with a Cu--Zn separation of 2.942(2) Å. Further, the acetate group bridges the two metal ions providing a five-coordinate geometry about both metal ions. The CuM complexes except for the CuZn complex show significant antiferromagnetic spin-exchange within each dinuclear unit. The CuNi complex shows the ESR spectrum of the spin-doublet ground state which demonstrates the delocalization of the unpaired electron over the CuNi core.

Introduction

Heterodinuclear metal complexes having two different metal ions in close proximity are of interest because of the unique physicochemical properties that arise from metal−metal interaction.[1−3] In particular, the recent recognition of heterodinuclear cores at the active sites of purple acid phosphatase (FeZn),[4] human calcineurin (FeZn),[5] and human protein phosphatase 1 (MnFe)[6] has stimulated interest in functions of heterodinuclear metal complexes. In order to provide discrete heterodinuclear core complexes phenol-based dinucleating macrocycles with two dissimilar metal-binding sites, sharing two phenolic oxygens, have been developed.[7−13] This type of dinucleating macrocycle shown in Chart 1 is distinguished from

Chart 1

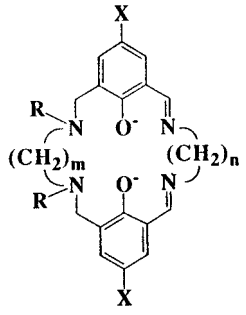

others in that the two metal-binding sites differ from each other with respect to the saturation or unsaturation of the donor nitrogen, but the availability of such macrocycles is still limited[11−13] because of the difficulty in preparation. A macrocycle bearing a pyridyl pendant group on each amine nitrogen was synthesized by Fraser et al.,[12] but their synthesis necessitates many elaborate steps. Thus, it is of value to establish a facile synthetic method applicable to a wide range of macrocycles of this type.

[⊗] Abstract published in *Advance ACS Abstracts,* May 15, 1997.

(1) Kahn, O. *Struct. Bonding (Berlin)* **1987**, *68*, 89.
(2) Zanello, P.; Tamburini, S.; Vigato, P. A.; Mazzocchin, G. A. *Coord. Chem. Rev.* **1987**, *77*, 165.
(3) Vigato, P. A.; Tamburini, S.; Fenton, D. E. *Coord. Chem. Rev*. **1990**, *106*, 25.
(4) Sträter, N.; Klabunde, T.; Tucker, P.; Witzel, H.; Krebs, B. *Science* **1995**, *268*, 1489.
(5) Kissinger, C. R.; Parge, H. E.; Knighton, D. R.; Lewis, C. T.; Pelletier, L. A.; Tempczyk, A.; Kalish, V. J.; Tucker, K. D.; Showalter, R. E.; Moomaw, E. W.; Gastinel, L. N.; Habuka, N.; Chen, X.; Maldonado, F.; Barker, J. E.; Bacquet, R.; Villafranca, J. E. *Nature (London)* **1995**, *378*, 641.
(6) Egloff, M-P.; Cohen, P. T. W.; Reinemer, P.; Barford, D. *J. Mol. Biol*. **1995**, *254*, 942.
(7) Ōkawa, H.; Kida, S. *Inorg. Nucl. Chem. Lett*. **1971**, *7*, 751. Ōkawa, H.; Kida, S. *Bull. Chem. Soc. Jpn.* **1972**, *45*, 1759.
(8) Tadokoro, M.; Ōkawa, H.; Matsumoto, N.; Koikawa, M.; Kida, S. *J. Chem. Soc., Dalton Trans*. **1991**, 1657. Tadokoro, M.; Sakiyama, H.; Matsumoto, N.; Kodera, M.; Ōkawa, H.; Kida, S. *Ibid*. **1992**, 313.

S0020-1669(96)01443-7 CCC: $14.00

In this study a macrocycle of this type (X = Br, R = CH_3, $m = 2$ and $n = 3$; abbreviated as H_2L) has been obtained as a dinuclear Cu(II)Pb(II) complex $[CuPb(L)](ClO_4)_2$. An analogous complex $[CuPb(L)(dmf)(BzO)]ClO_4$ ($BzO^- = C_6H_5COO^-$) has been structurally characterized and shows that the Cu(II) is bonded to the $N(imine)_2O_2$ site and the Pb(II) is bonded to the $N(amine)_2O_2$ site. $[CuPb(L)](ClO_4)_2$ reacts with metal(II) sulfate salts providing $Cu^{II}M^{II}$ complexes $[CuM(L)](ClO_4)_2 \cdot nH_2O$ (M = Mn ($n = 2$) (**1**), Co ($n = 2$) (**2**), Ni ($n = 0$) (**3**), Cu ($n = 0$) (**4**), Zn ($n = 1$) (**5**)). X-ray crystallography for an analogous CuZn complex, $[CuZn(L)(AcO)]ClO_4$ ($AcO^- = CH_3COO^-$), has proved that the Cu(II) is now bound at the $N(amine)_2O_2$ site and that the Zn(II) occupies the $N(imine)_2O_2$ site. The cryomagnetic (4.2−300 K) and electrochemical properties of the CuM complexes (**1**−**5**) are studied; in particular the electronic property of the spin-doublet state of the CuNi complex is examined by means of ESR spectroscopy.

In the course of this study Karunakaran and Kandaswamy[13] reported related macrocycles containing the piperazine entity instead of the $-N(CH_3)CH_2CH_2N(CH_3)-$ part of our macrocycle. They studied dinuclear copper(II) complexes but not heterodinuclear complexes of their ligands. A part of this work was preliminarily reported.[11]

Experimental Section

Physical Measurements. Elemental analyses of C, H, and N were obtained at The Service Center of Elemental Analysis of Kyushu University. Metal analyses were made on a Shimadzu AA-680 atomic absorption/flame emission spectrophotometer. Infrared spectra were recorded on a JASCO IR-810 spectrophotometer using KBr disks. ^{1}H-NMR spectra (400 MHz) were measured on a JEOL JNM-GX 400 spectrometer in $CDCl_3$, using tetramethylsilane as the internal standard. Electronic absorption spectra in *N*,*N*-dimethylformamide (DMF) or dimethyl sulfoxide (DMSO) and reflectance spectra were recorded on a Shimadzu MPS-2000 spectrophotometer. Molar conductances were measured in DMF and DMSO with a DKK AOL-10 conductivity meter at room temperature. Magnetic susceptibilities of powdered samples were measured on a Hoxan HSM-D SQUID susceptometer in the temperature range 4.2−80 K (applied magnetic field of 100 G) and a Faraday balance in the range 80−290 K (applied field of 3000 G). Calibrations[14] were made with $Mn(NH_4)_2(SO_4)_2 \cdot 6H_2O$ for the SQUID susceptometer and with $[Ni(en)_3]S_2O_3$ (en = ethylenediamine) for the Faraday balance. Diamagnetic corrections for the constituting atoms were made by the use of Pascal's constants.[15] X-band ESR spectra were recorded on a JEOL JEX-FE3X spectrometer on frozen DMF solution at liquid-nitrogen temperature. Cyclic voltammograms were measured using a BAS CV-50W electrochemical analyzer in DMSO solution containing tetra-*n*-butylammonium perchlorate (TBAP) as the supporting electrolyte. A three-electrode cell was used which was equipped with a glassy carbon working electrode, a platinum coil as the counter electrode, and a Ag/Ag^+ (TBAP/acetonitrile) reference electrode. (*Caution! TBAP is explosive and should be handled with great care*). Controlled-potential coulometric experiments were made on an apparatus comprising an HA-501 potentiostat/galvanostat, an HB-104 function generator, and an HF-201 coulomb/amperemeter from Hokuto Denko Ltd.

Preparation. *N*,*N*′-Dimethyl-*N*,*N*′-ethylenebis(5-bromo-3-formyl-2-hydroxybenzylamine) (H_2L'). *N*,*N*′-Dimethylethylenediamine (4.4 g, 50 mmol), 5-bromosalicylaldehyde (20.0 g, 100 mmol), and paraformaldehyde (4.0 g, 134 mmol) were dissolved in ethanol (300 cm^3), and the mixture was refluxed for 1 week to form a white powder. It was separated by filtration, washed with ethanol, and dried in vacuo. It melts at 184−185 °C. The yield was 10.4 g (51%). ^{1}H-NMR (δ/ppm in $CDCl_3$): 2.30 (s, 6H, N−CH_3), 2.70 (s, 4H, $-CH_2CH_2-$), 3.68 (s, 4H, Ar−CH_2−N), 7.71 (s, 2H, ring proton), 7.72 (s, 2H, ring proton), 10.18 (s, 2H, −CHO). Selected IR data (ν/cm^{-1} using KBr): 1680.

[Cu(L′)]. H_2L' (0.5 g, 1 mmol) was dissolved in an aqueous solution of potassium hydroxide (0.11 g, 2 mmol). To the resulting yellow solution was added dropwise an aqueous solution of copper(II) acetate monohydrate (0.2 g, 1 mmol) to form [Cu(L′)] as a green precipitate. It was collected by suction filtration, washed successively with water and ether, and dried in vacuo. The yield was nearly quantitative. Selected IR data (ν/cm^{-1} using KBr): 1650. UV−vis [λ_{max}/nm (ϵ/M^{-1} cm^{-1})]: 386 (13 700), 660 (270) in DMF; 387 (14 500), 660 (290) in DMSO; 377, 385, 585 on a powdered sample.

[CuPb(L)](ClO$_4$)$_2$. To a hot suspension of [Cu(L′)] (0.58 g, 1 mmol) in a chloroform−methanol mixture (15:85 in volume, 30 cm^3) was added a methanol solution of lead(II) perchlorate trihydrate (0.47 g, 1 mmol). To the resulting green solution was added dropwise a methanol solution (10 cm^3) of 1,3-diaminopropane (0.10 g, 1 mmol) to give a dark-green powder. It was collected by suction filtration, washed with diethyl ether, and dried in vacuo. The yield was nearly quantitative. μ_{eff} per CuPb: 1.77 μ_B at 290 K. Selected IR data (ν/cm^{-1} using KBr): 1618, 1440, 1285, 1102, 1090, 1057, 618. UV−vis [λ_{max}/nm (ϵ/M^{-1} cm^{-1})]: 360 (6720), 642 (132) in DMF; 360 (7160), 647 (130) in DMSO; 357, 607 on a powdered sample. Molar conductance (Λ_M/S $cm^2 mol^{-1}$): 112 in DMF; 62 in DMSO.

A portion of the complex was dissolved in DMF and mixed with an aqueous solution containing a slight excess of sodium benzoate. The diffusion of diethyl ether resulted in the precipitation of brown microcrystals. They were recrystallized from a DMF/ether mixture to form large single crystals of $[CuPb(L)(BzO)(DMF)]ClO_4$ suitable for X-ray crystallography. μ_{eff} per CuPb: 1.82 μ_B at 290 K. Selected IR data (ν/cm^{-1} using KBr): 1655, 1610, 1445, 1390, 1320, 1090, 620. UV−vis [λ_{max}/nm (ϵ/M^{-1} cm^{-1})]: 365 (9700), 600 (57) in DMF; 367 (9850), 610 (70)) in DMSO; 365, 576, 660 sh on a powdered sample. Molar conductance (Λ_M/S cm^2 mol^{-1}): 58 in DMF; 29 in DMSO.

[CuMn(L)](ClO$_4$)$_2$·2H$_2$O (1). To a suspension of $[CuPb(L)](ClO_4)_2$ (0.60 g, 0.6 mmol) in dry acetonitrile (20 cm^3) was added a dry methanol solution (10 cm^3) of manganese(II) sulfate hexahydrate (0.15 g, 0.6 mmol), and the mixture was stirred at ambient temperature for 3 h to result in the precipitation of $PbSO_4$. It was removed by filtration, and the filtrate was evaporated to dryness. The residue was extracted with dry acetonitrile, and the extract was filtered once to separate $PbSO_4$. This operation (dissolution in acetonitrile and filtration) was repeated three times, and the acetonitrile solution was diffused with diethyl ether to give a dark-green precipitate. The yield was 0.14 g (25%). Selected IR data (ν/cm^{-1} using KBr): 1625, 1450, 1295, 1100, 1065, 620 μ_{eff} per CuMn: 5.48 μ_B at 290 K. UV−vis [λ_{max}/nm (ϵ/M^{-1} cm^{-1})]: 345 (10 700), 635 (150) in DMF; 346 (10 700), 651 (150) in DMSO; 348, 570 on a powdered sample. Molar conductance (Λ_M/S cm^2 mol^{-1}): 133 in DMF; 66 in DMSO.

[CuCo(L)](ClO$_4$)$_2$·2H$_2$O (2). This complex was obtained as green microcrystals (yield: 31%). Selected IR data (ν/cm^{-1} using KBr): 1620, 1450, 1295, 1100, 620. μ_{eff} per CuCo: 4.10 μ_B at 290 K. UV−vis [λ_{max}/nm (ϵ/M^{-1} cm^{-1})]: 345 (9690), 565 br (210), 610 sh (200) in DMF; 345 (9310), 571 (170), 612 sh (163) in DMSO; 350, 570 on a powdered sample. Molar conductance (Λ_M/S cm^2 mol^{-1}): 138 in DMF; 60 in DMSO.

[CuNi(L)](ClO$_4$)$_2$ (3). Green microcrystals formed (yield: 35%). Selected IR data (ν/cm^{-1} using KBr): 1630, 1440, 1300, 1140, 1120, 1074, 620. μ_{eff} per CuNi: 2.78 μ_B at 290 K. UV−vis [λ_{max}/nm (ϵ/M^{-1} cm^{-1})]: 350 (10 500), 610 (180), 750 sh (75) in DMF; 350 (9300), 587 (154), 752 sh (∼50) in DMSO; 360, 570, 750 on a powdered sample. Molar conductance (Λ_M/S cm^2 mol^{-1}): 124 in DMF; 56 in DMSO.

(9) Ōkawa, H.; Nishio, J.; Ohba, M.; Tadokoro, M.; Matsumoto, N.; Koikawa, M.; Kida, S.; Fenton, D. E. *Inorg. Chem.* **1993**, *32*, 2949. Nishio, J.; Ōkawa, H.; Ohtsuka, S.; Tomono, M. *Inorg. Chim. Acta* **1994**, *218*, 27. Shimoda, J.; Furutachi, H.; Yonemura, M.; Ohba, M.; Matsumoto, N.; Ōkawa, H. *Chem. Lett*. **1996**, 979.
(10) Ohtsuka, S.; Kodera, M.; Motoda, K.; Ohba, M.; Ōkawa, H. *J. Chem. Soc., Dalton Trans*. **1995**, 2599.
(11) Yonemura, M.; Matsumura, Y.; Ohba, M.; Ōkawa, H.; Fenton, D. E. *Chem. Lett*. **1996**, 601.
(12) Fraser, C.; Johnston, L.; Rheingold, A. L.; Haggerty, B. S.; Williams, G. K.; Whelan, J.; Bosnich, B. *Inorg. Chem*. **1992**, *31*, 1835. McCollum, D. G.; Yap, G. P. A.; Rheingold, A. L.; Bosnich, B. *J. Am. Chem. Soc.* **1996**, *118*, 1365 and references therein.
(13) Karunakaran, S.; Kandaswamy, M. *J. Chem. Soc., Dalton Trans.* **1994**, 1595.
(14) Lindoy, L. F.; Katovic, V.; Busch, D. H. *J. Chem. Educ*. **1972**, *49*, 117.
(15) Boudreaux, E. A.; Mulay, L. N. *Theory and Applications of Molecular Paramagnetism*; Wiley: New York, 1976; p 491.

Table 1. Crystallographic Data for $[CuPb(L)(BzO)(dmf)]ClO_4$ and $[CuZn(L)(AcO)]ClO_4$

	complex	
	$[CuPb(L)(BzO)(dmf)]ClO_4$	$[CuZn(L)(AcO)]ClO_4$
formula	$C_{33}H_{38}Br_2ClCuN_5O_9Pb$	$C_{25}H_{29}Br_2ClCuN_4O_8Zn$
fw	1114.70	837.71
cryst color	brown	green
cryst size/mm^3	0.20 × 0.15 × 0.15	0.20 × 0.25 × 0.15
cryst system	triclinic	triclinic
space group	$P\bar{1}$ (No. 2)	$P\bar{1}$ (No. 2)
a/Å	13.998(2)	12.290(3)
b/Å	15.568(2)	13.402(4)
c/Å	8.699(2)	11.501(2)
α/deg	95.32(1)	95.10(2)
β/deg	92.23(1)	116.68(2)
γ/deg	82.81(1)	112.00(2)
V/Å^3	1871.9(5)	1491.8(9)
Z	2	2
D_{calcd}/g·cm^{-3}	1.978	1.865
μ(Mo Kα)/cm^{-1}	73.38	43.47
no. of reflcns ($I > 3.00\sigma(I)$)	3788	2497
F(000)	1082	834
R^a/%	0.058	0.046
$R_w^{b,c}$/%	0.069	0.034

[a] $R = \sum||F_o| - |F_c||/\sum|F_o|$. [b] $R_w = [\sum w(|F_o| - |F_c|)^2/\sum w|F_o|^2]^{1/2}$. [c] $w = 1/\sigma(|F_o|)^2$.

$[CuCu(L)](ClO_4)_2$ (4). Green microcrystals formed (yield: 50%). Selected IR data (ν/cm^{-1} using KBr): 1625, 1455, 1300, 1100, 625. μ_{eff} per Cu: 0.79 μ_B at 290 K. UV−vis [λ_{max}/nm (ϵ/M^{-1} cm^{-1})]: 345 (9870), 620 (200) in DMF; 346 (10 300), 639 (208) in DMSO; 340, 570 on a powdered sample. Molar conductance (Λ_M/S cm^2 mol^{-1}): 134 in DMF; 61 in DMSO.

$[CuZn(L)](ClO_4)_2 \cdot H_2O$ (5). A green powder formed (yield: 60%). Selected IR data (ν/cm^{-1} using KBr): 1625, 1450, 1300, 1100, 620. μ_{eff} per CuZn: 1.77 μ_B at 290 K. UV−vis [λ_{max}/nm (ϵ/M^{-1} cm^{-1})]: 350 (10 200), 625 (120) in DMF; 349 (10 500), 639 (120) in DMSO; 340, 570 on a powdered sample. Molar conductance (Λ_M/S cm^2 mol^{-1}): 126 in DMF; 66 in DMSO.

$[CuZn(L)(AcO)]ClO_4$ (5′). A dry methanol solution (10 cm^3) of zinc(II) sulfate heptahydrate (0.17 g, 0.6 mmol) was added to a suspension of $[CuPb(L)](ClO_4)_2$ (0.61 g, 0.6 mmol) and sodium acetate trihydrate (0.08 g, 0.6 mmol) in dry acetonitrile (20 cm^3), and the mixture was stirred at ambient temperature for 3 h to result in the precipitation of $PbSO_4$. It was removed by filtration, and the filtrate was evaporated to dryness. The residue was extracted with DMF, and the extract was filtered once to separate insoluble materials. The filtrate was diffused with diethyl ether to give green single crystals. The yield was 0.15 g (30%). μ_{eff} per CuZn: 1.78 μ_B at 290 K. Selected IR data (ν/cm^{-1} using KBr): 1625, 1575, 1450, 1400, 1300, 1100, 620. UV−vis [λ_{max}/nm (ϵ/M^{-1} cm^{-1})]: 353 (10 600), 627 (105) in DMF; 352 (10 900), 624 (103) in DMSO; 354, 646 on a powdered sample. Molar conductance (Λ_M/S cm^2 mol^{-1}): 60 in DMF; 28 in DMSO.

Crystal Structure Determination of $[CuPb(L)(BzO)(dmf)]ClO_4$ and $[CuZn(L)(AcO)]ClO_4$. All the crystallographic measurements were made on a Rigaku AFC7R diffractometer with graphite-monochromated Mo Kα radiation (λ = 0.710 69 Å) and a 12 kW rotating anode generator. The data were collected at 20 ± 1 °C. Cell constants and an orientation matrix for the data collection were obtained from 25 reflections in the range $20.92 < 2\theta < 23.91°$ for the CuPb complex and from 23 reflections in the range $20.15 < 2\theta < 23.63°$ for the CuZn complex. For the intensity collections, the $\omega-2\theta$ scan mode was used to a maximum 2θ value of 45.0° for the CuPb complex and 50.0° for the CuZn complex at a scan speed of 16.0°/min (in ω). The octant measured was $+h,+k,\pm l$ for both complexes. Pertinent crystallographic parameters are summarized in Table 1.

A total of 5144 reflections for the CuPb complex and 5594 reflections for the CuZn complex were collected. Three standard reflections were monitored every 150 measurements. Over the course of data collection, the standards decresed by 0.7% for the CuPb complex and 0.6% for the CuZn complex. A linear correction factor was applied to the data to account for the phenomena. An empirical absorption correction based on azimuthal scans of several reflections was applied which resulted in transmission factors ranging from 0.60 to 1.00 for the CuPb complex and from 0.70 to 1.00 for the CuZn complex. Reflection data were corrected for Lorentz and polarization effects.

The structures were solved by direct method and expanded using Fourier techniques. The non-hydrogen atoms were refined anisotropically except for the dmf molecule in the CuPb complex. The dmf molecule showed a disorder around its oxygen so that constituting atoms were refined as rigid groups. Hydrogen atoms were included in the structure factor calculation but not refined. Neutral atom scattering factors were taken from Cromer and Waber.[16] Anomalous dispersion effects were included in the final calculations;[17] the values for $\Delta f'$ and $\Delta f''$ were taken from ref 18, and those for the mass-attenuation coefficients from ref 19. Computations were carried out on an IRIS Indigo computer using the teXsan crystallographic software package of Molecular Structure Corporation.[20]

Results and Discussion

Precursor CuPb Complex. Preparation. The two N_2O_2 metal-binding sites of the macrocycle $(L)^{2-}$ share the two phenolic oxygens but are not equivalent with respect to the aminic or iminic nature of the donor nitrogens. In order to prepare such unsymmetrical macrocycles it is recommended to use an appropriate acyclic precursor in the template reaction. For the present purpose acyclic *N,N′*-dimethyl-*N,N′*-ethylenebis-(5-bromo-3-formyl-2-hydroxybenzylamine) (H_2L') was adopted as the precursor, which was obtained in a tolerable yield by the Mannich reaction of 5-bromosalicylaldehyde, paraformaldehyde, and *N,N′*-dimethylethylenediamine in ethanol. In its copper(II) complex [Cu(L′)] the Cu ion is bound at the $N(amine)_2O_2$ site judged from the presence of a ν(CO) (formyl) mode at 1650 cm^{-1} in the IR spectrum. The reaction of [Cu(L′)] with 1,3-diaminopropane in the presence of lead(II) perchlorate trihydrate formed a Cu(II)Pb(II) complex $[CuPb(L)](ClO_4)_2$.

Crystal Structure of $[CuPb(L)(BzO)(dmf)]ClO_4$. The benzoate derivative $[CuPb(L)(BzO)(dmf)]ClO_4$ formed good single crystals suitable for X-ray crystallography. The ORTEP[21] view of the cation is shown in Figure 1. Relevant bond distances and angles are given in Table 2.

The cation is comprised of $(L)^{2-}$, one Cu(II) and one Pb(II) ion, one benzoate group, and one dmf molecule; the perchlorate ion is free from coordination. The Cu(II) resides at the $N(imine)_2O_2$ site and the Pb(II) at the $N(amine)_2O_2$ site, demonstrating that a migratory transmetalation has occurred and that the Cu(II) is shifted from the $N(amine)_2O_2$ site of $(L')^{2-}$ to the $N(imine)_2O_2$ site of $(L)^{2-}$ in the cyclization process. The two metal ions are bridged by the phenolic oxygens O(1) and O(2) with an intermetallic separation of 3.466(2) Å. The {$CuN(imine)_2O_2$} chromophore involving the aromatic moieties is nearly coplanar. The Cu−N and Cu−O bond distances fall in the range 1.92(1)−2.00 (1) Å. The N(3)−Cu−N(4) bond angle (99.8(6)°) is significantly larger than 90°, and the O(1)−Cu−O(2) angle (78.7(5)°) is smaller than 90°.

The Pb(II) at the $N(amine)_2O_2$ site is significantly deviated from the least-squares $N(amine)_2O_2$ plane and assumes a seven-coordinate geometry together with the bidentate benzoate oxygens (O(3) and O(4)) and a dmf oxygen (O(5)). The least-squares $N(amine)_2O_2$ and $N(imine)_2O_2$ planes are bent at the

(16) Cromer, D. T.; Waber, J. T. *International Tables for X-ray Crystallography*; Kynoch Press: Birmingham, U.K., 1974; Vol. IV.
(17) Ibers, J. A.; Hamilton, W. C. *Acta Crystallogr.* **1964**, *17*, 781.
(18) Creagh, D. C.; McAuley, W. J. *International Tables for Crystallography*; Wilson, A. J. C., et al., Eds.; Kluwer Acad. Pub.; Boston, MA, 1992; pp 219−222.
(19) Creagh, D. C.; Hubbell, J. H. *International Tables for Crystallography*; Wilson, A. J. C., et al., Eds.; Kluwer Acad. Pub.; Boston, MA, 1992; pp 200−206.
(20) TEXSAN, Molecular Structure Corp., Houston, TX, 1985.
(21) Johnson, C. K. Report 3794, Oak Ridge National Laboratory, Oak Ridge, TN, 1965.

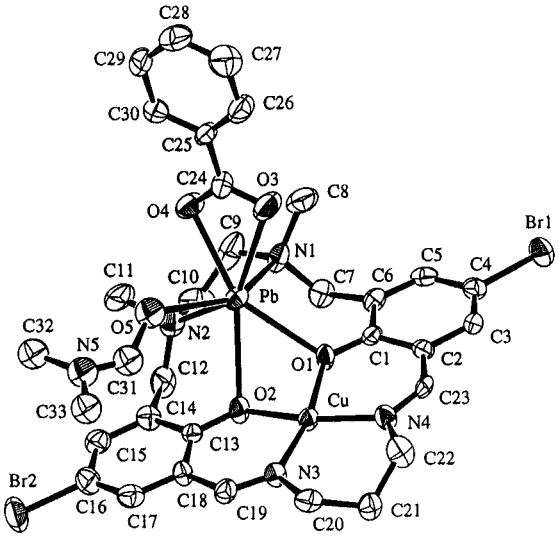

Figure 1. ORTEP view of the cationic part of [CuPb(L)(BzO)(dmf)]-ClO4.

Table 2. Selected Bond Distances and Angles for $[CuPb(L)(BzO)(dmf)]ClO_4$

Bond Distances (Å)			
Cu−O(1)	1.92(1)	Pb−O(3)	2.61(1)
Cu−O(2)	1.93(1)	Pb−O(4)	2.52(1)
Cu−N(3)	1.96(1)	Pb−O(5)	2.7702(9)
Cu−N(4)	2.00(1)	Pb−N(1)	2.56(2)
Pb−O(1)	2.62(1)	Pb−N(2)	2.56(2)
Pb−O(2)	2.70(1)	Cu···Pb	3.466(2)
Bond Angles (deg)			
Cu−O(1)−Pb	98.4(5)	O(2)−Pb−O(4)	154.2(4)
Cu−O(2)−Pb	95.5(5)	O(2)−Pb−O(5)	87.6(3)
O(1)−Cu−O(2)	78.7(5)	O(2)−Pb−N(1)	107.2(5)
O(1)−Cu−N(3)	167.4(6)	O(2)−Pb−N(2)	73.4(4)
O(1)−Cu−N(4)	90.3(6)	O(3)−Pb−O(4)	50.9(4)
O(2)−Cu−N(3)	91.3(6)	O(3)−Pb−O(5)	93.2(4)
O(2)−Cu−N(4)	168.9(6)	O(3)−Pb−N(1)	84.7(6)
N(3)−Cu−N(4)	99.8(6)	O(3)−Pb−N(2)	134.4(5)
O(1)−Pb−O(2)	54.6(4)	O(4)−Pb−O(5)	76.9(4)
O(1)−Pb−O(3)	107.4(4)	O(4)−Pb−N(1)	80.1(5)
O(1)−Pb−O(4)	148.5(4)	O(4)−Pb−N(2)	85.7(5)
O(1)−Pb−O(5)	132.0(3)	O(5)−Pb−N(1)	151.8(3)
O(1)−Pb−N(1)	74.8(4)	O(5)−Pb−N(2)	89.1(4)
O(1)−Pb−N(2)	104.4(5)	N(1)−Pb−N(2)	73.0(5)
O(2)−Pb−O(3)	152.2(4)		
Dihedral Angles (deg)			
O(1)O(2)N(1)N(2)−O(1)O(2)N(3)N(4)			165.13

O(1)--O(2) edge with a dihedral angle of 14.87°. The Pb−N and Pb−O bond distances fall in the range 2.52(1)−2.77(1) Å. The amino nitrogens N(1) and N(2) have the *R* and *S* configuration, respectively, as found for [Cu(L)];[11] the two methyl groups attached to the nitrogen atoms are cis to each other. The trimethylene lateral chain assumes the chair conformation.

Dinuclear CuM Complexes. Preparation. The CuPb complex $[CuPb(L)](ClO_4)_2$ is a good precursor for the heterodinuclear $Cu^{II}M^{II}$ complexes **1**−**5**. The transmetalation of the Pb(II) ion for a transition M(II) ion could be successfully achieved by the reaction of $[CuPb(L)](ClO_4)_2$ with a metal(II) sulfate salt in acetonitrile. In this reaction Pb(II) is eliminated from the reaction mixture as insoluble $PbSO_4$.

Crystal Structure of $[CuZn(L)(AcO)]ClO_4$. X-ray crystallographic studies have been made for the acetate derivative of the CuZn complex $[CuZn(L)(AcO)]ClO_4$. An ORTEP view of the complex cation is shown in Figure 2; selected bond distances and angles are given in Table 3.

The cation is comprised of $(L)^{2-}$, one Cu(II), one Zn(II), and one acetate ion. It is found that the Cu(II) resides at the

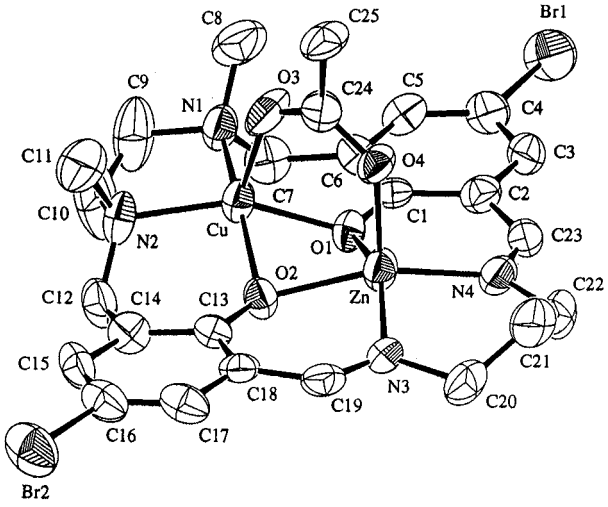

Figure 2. ORTEP view of the cationic part of $[CuZn(L)(AcO)]ClO_4$.

Table 3. Selected Bond Distances and Angles for $[CuZn(L)(AcO)]ClO_4$

Bond Distances (Å)			
Cu−O(1)	1.990(6)	Zn−O(2)	2.061(6)
Cu−O(2)	1.973(6)	Zn−O(4)	2.018(6)
Cu−O(3)	2.093(7)	Zn−N(3)	2.033(8)
Cu−N(1)	2.026(8)	Zn−N(4)	2.029(8)
Cu−N(2)	2.017(7)	Cu···Zn	2.942(2)
Zn−O(1)	2.059(6)		
Bond Angles (deg)			
Cu−O(1)−Zn	93.2(2)	N(1)−Cu−N(2)	88.3(3)
Cu−O(2)−Zn	93.6(2)	O(1)−Zn−O(2)	73.6(2)
O(1)−Cu−O(2)	77.1(2)	O(1)−Zn−O(4)	101.9(2)
O(1)−Cu−O(3)	98.2(2)	O(1)−Zn−N(3)	151.1(3)
O(1)−Cu−N(1)	94.2(3)	O(1)−Zn−N(4)	88.0(3)
O(1)−Cu−N(2)	153.8(3)	O(2)−Zn−O(4)	103.1(2)
O(2)−Cu−O(3)	98.0(3)	O(2)−Zn−N(3)	87.7(3)
O(2)−Cu−N(1)	161.7(3)	O(2)−Zn−N(4)	150.2(3)
O(2)−Cu−N(2)	92.7(3)	O(4)−Zn−N(3)	103.8(3)
O(3)−Cu−N(1)	99.2(3)	O(4)−Zn−N(4)	103.4(3)
O(3)−Cu−N(2)	107.1(3)	N(3)−Zn−N(4)	98.8(3)
Dihedral Angles (deg)			
O(1)O(2)N(1)N(2)−O(1)O(2)N(3)N(4)			163.57

$N(amine)_2O_2$ site and the Zn(II) at the $N(imine)_2O_2$ site. The pair of metal ions are bridged by the two phenolic oxygens and the acetate group, providing a distorted five-coordinate geometry for both metal ions. The Cu--Zn separation is 2.942(2) Å.

Our assignments of the positions of the metal ions are based on the relative metal−N(O) bond distances and the geometric features of the two chromophores. The $\{CuN(amine)_2O_2\}$ site is close to square-pyramidal (the geometric parameter τ[22] is 0.13). The basal Cu−ligand bond distances fall in the range 1.973(6)−2.026(8) Å, and the axial Cu−O(3) bond is elongated (2.093(7) Å) owing to the Jahn−Teller effect in d^9 electronic configuration. The deviation of the Cu from the basal N_2O_2 least-squares plane toward O(3) is 0.373 Å. The $\{ZnN(imine)_2O_2\}$ site is very close to square-pyramidal (τ: 0.015) with basal Zn−O and Zn−N bond distances (2.029(8)−2.061(6) Å) which are longer than the corresponding Cu−O and Cu−N distances of $\{CuN(amine)_2O_2\}$ in accord with the relative size of Cu(II) and Zn(II) ions.[23] Instead, the apical Zn−O(4) distance is short (2.018 Å). Because of the acetate bridge, the $N(amine)_2O_2$ and the $N(imine)_2O_2$ least-squares planes are bent at the O1--O2 edge with a dihedral angle of 16.43°. The

(22) Addison, A. W.; Rao, T. N.; Reedijk, J.; Rijn, J. V.; Verschoor, G. C. *J. Chem. Soc., Dalton Trans.* **1984**, 1349.
(23) Shannon, R. D.; Prewitt, C. T. *Acta Crystallogr.* **1969**, *B25*, 925. Shannon, R. D. *Ibid.* **1976**, *A32*, 751.

Scheme 1

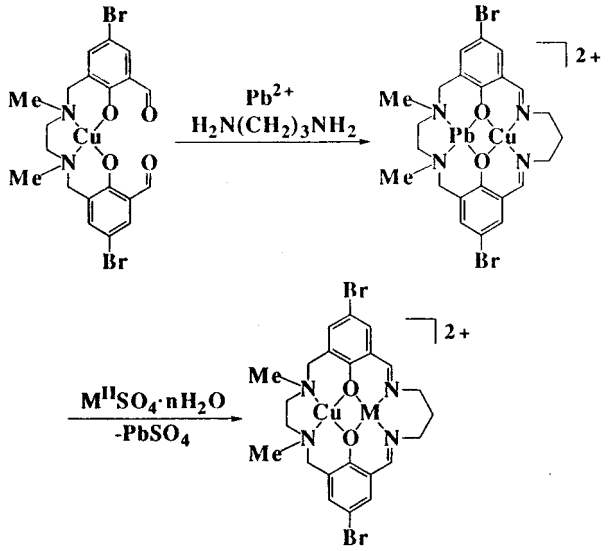

deviation of the Zn from the basal N_2O_2 least-squares plane toward O(4) is very large (0.463 Å).

X-ray crystallography has established the migration of the Cu(II) ion from the N(imine)$_2$O$_2$ site in the CuPb complex to the N(amine)$_2$O$_2$ site in the CuZn complex (see Scheme 1). The driving force in the initial reaction involving Cu(II) and Pb(II) may be related to the nature of the donor compartments. The Cu(II) migrates to occupy the relatively rigid N(imine)$_2$O$_2$ site, which provides the more preferred square coplanar environment, and the larger Pb(II) is then accommodated in the more flexible N(amine)$_2$O$_2$ site. The site selectivity observed in the CuZn complex shows that a reversal of the migratory transmetalation has occurred with the Cu(II) reverting to the N(amine)$_2$O$_2$ site. This process may be related to the relative sizes of the metal ions and the metal-binding cavities. That is, the N(amine)$_2$O$_2$ site, which is the smaller in cavity size, accomodates the smaller Cu(II) ion and the N(imine)$_2$O$_2$ site accomodates the larger Zn(II) ion. The N(amine)$_2$O$_2$ site is also the more flexible and so able to accommodate any distortions imposed at Cu(II) by the Jahn−Teller effect. Similarly, for the other complexes **1**−**4** the Cu(II) ion always occupies the N(amine)$_2$O$_2$ site and the M(II) ion at the N(imine)$_2$O$_2$ site, as judged from visible spectral similarity (see below).

Electronic and Infrared Spectra. The CuM complexes (**1**−**5**) are stable in DMF and DMSO and behave as 2:1 electrolytes in both solvents (124−138 Λ_M/S cm^2 mol^{-1} in DMF and 56−66 Λ_M/S cm^2 mol^{-1} in DMSO). Electronic spectral data for the complexes are given in the Experimental Section. An intense band around 345−350 nm is commonly seen for all the complexes which is assigned to the $\pi-\pi^*$ transition associated with the azomethine linkages.[24] The CuMn (**1**) and CuZn (**5**) complexes show one visible band around ∼630 nm that is assigned to a superposed band of d−d transitions of the Cu(II) ion. The CuCu complex (**4**) also has one visible band around 620 nm whose extinction coefficient is large relative to those of **1** and **5**. The CuCo complex (**4**) shows an additional band at 565 nm as a discernible shoulder that is assigned to a d−d compoment of the Co(II) ion. Similarly the CuNi complex (**3**) shows a d−d compoment of the Ni(II) near ∼750 nm.

In the macrocyclic complex [CuPb(L)](ClO$_4$)$_2$ the intense ν(C═N) band appears at 1618 cm^{-1}. The ν(C═N) band of the dinuclear CuM complexes **1**−**5** is observed around 1620−1630 cm^{-1}. For **1**, **2**, **4,** and **5** the ν_3 and ν_4 modes of perchlorate ion are seen as unsplit band at ∼1100 and ∼620 cm^{-1}, respectively. In the case of the CuNi complex **3** the ν_3 mode splits into 1140, 1120, and 1075 cm^{-1}. This fact implies the axial coordination of the perchlorate ions.[25]

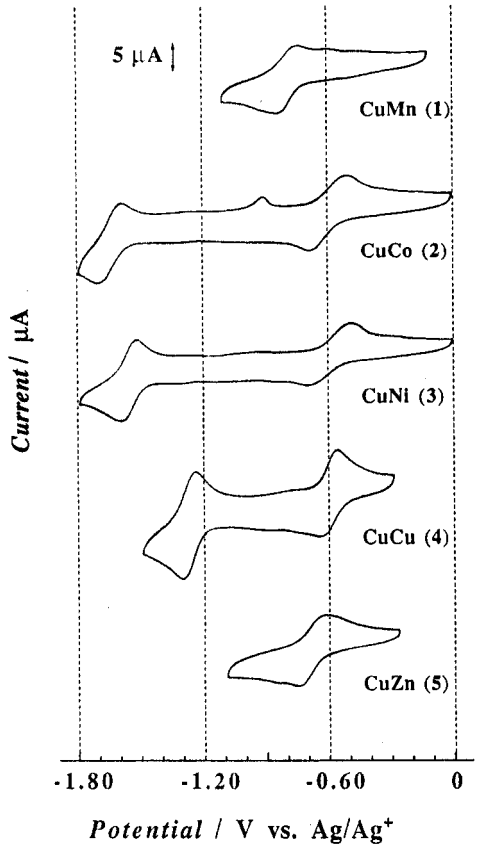

Figure 3. Cyclic voltammograms of the complexes **1**−**5**.

Electrochemical Properties. All the CuM complexes **1**−**5** showed good electrode stability in DMSO. The cyclic voltammograms in this solvent are shown in Figure 3, and the numerical data are summarized in Table 4.

The CuMn complex (**1**) shows a quasi-reversible couple at −0.78 V (vs Ag/Ag$^+$). Similarly, the CuZn complex (**5**) shows a quasi-reversible couple at −0.69 V. This couple can be attributed to the reduction occurring at the Cu(II) center.[26] For the CuCo (**2**) and CuNi (**3**) complexes two quasi-reversible couples are observed. The first couple near −0.6 V is attributed to the reduction occurring at the Cu(II) center, and the second couple at lower potential, to the reduction at the M(II) center. The CuCu complex (**4**) also shows two redox couples at −0.60 and −1.28 V. In this case it is not obvious if the first reduction occurs at the Cu(II) at the N(amine)$_2$O$_2$ site or the Cu(II) at the N(imine)$_2$O$_2$ site.

In order to provide unambiguous assignment of the redox couples coulometry studies were made at −0.4 V vs SCE (=−0.65 V vs Ag/Ag$^+$). The electric current observed corresponded to a one-electron reduction, and the resulting green solution showed ESR signals of $g_{\|} = 2.25$, $g_{\perp} = 2.01$ and $A_{\|} = 178 \times 10^{-4}$ cm^{-1} (frozen DMF solution at liquid-nitrogen temperature). This result clearly indicates the formation of a mixed-valence Cu^ICu^{II} complex of class I in the classification by Robin and Day.[27] The electronic absorption spectrum of the mixed-valence complex is characterized by a d−d transition band at 670 nm which is compared to that of [Cu(L′)] (660 nm) but not [Cu-

(24) Bosnich, B. *J. Am. Chem. Soc.* **1968**, *90*, 627.

(25) Nakamoto, K. *Infrared Spectra of Inorganic and Coordination Compounds;* Wiley Interscience: New York, 1970; p 175.

(26) Ōkawa, H.; Tadokoro, M.; Aratake, Y.; Ohba, M.; Shindo, K.; Mitsumi, M.; Koikawa, M.; Tomono, M.; Fenton, D. E. *J. Chem. Soc., Dalton Trans.* **1993**, 253.

(27) Robin, M. B.; Day, P. *Adv. Inorg. Chem. Radiochem.* **1967**, *10*, 247.

Table 4. Electrochemical Data for $Cu^{II}M^{II}$ Complexes in DMSO[a]

complexes	E_{pa}	E_{pc}	$E_{1/2}$ (ΔE[b])	E_{pa}	E_{pc}	$E_{1/2}$ (ΔE[b])
[CuMn(L)] (**1**)	−0.74	−0.82	−0.78 (0.08)			
[CuCo(L)] (**2**)	−0.51	−0.67	−0.59 (0.16)	−1.60	−1.69	−1.64 (0.08)
[CuNi(L) (**3**)	−0.49	−0.70	−0.60 (0.21)	−1.53	−1.59	−1.56 (0.06)
[CuCu(L)] (**4**)	−0.56	−0.63	−0.60 (0.07)	−1.25	−1.31	−1.28 (0.06)
[CuZn(L)] (**5**)	−0.63	−0.75	−0.69 (0.12)			

[a] Unit: V vs Ag/Ag^+. Conditions: glassy-carbon working, Pt auxiliary, and Ag/Ag^+ (TBAP/MeCN) reference electrodes. Supporting electrolyte: TBAP. Scan rate: 100 mV/s. Concentration: complex (1×10^{-3} M), TBAP (1×10^{-1} M) in DMSO. [b] $\Delta E = |E_{pa} - E_{pc}|$.

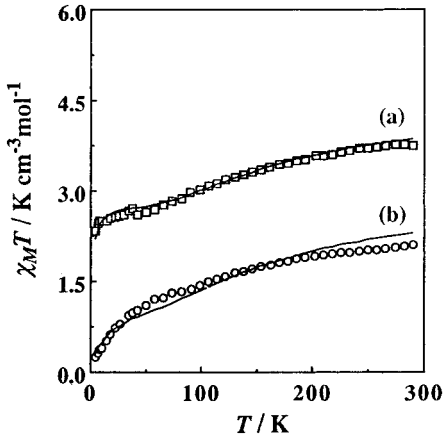

Figure 4. $\chi_M T$ vs T plots for (a) CuMn complex **1** and (b) CuCo complex **2**.

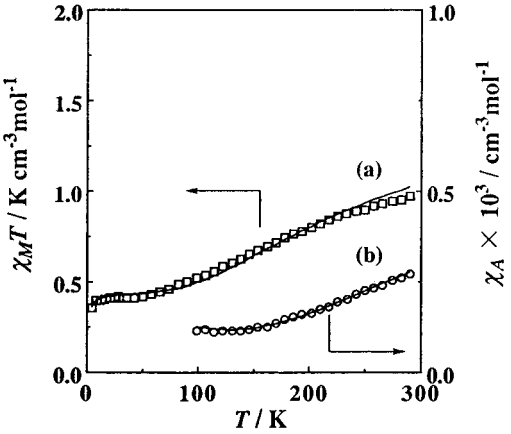

Figure 5. $\chi_M T$ vs T plots for CuNi complex **3** (a) and χ_A vs T plots for CuCu complex **4** (b).

(L)] (600 nm).[11] This fact strongly suggests that the Cu(II) at the $N(imine)_2O_2$ site is first reduced followed by the Cu(II) at the $N(amine)_2O_2$ site.

Magnetic Properties. The CuZn complex **5** has a normal magnetic moment for one unpaired electron. The other complexes **1**−**4** show a subnormal magnetic moment at room temperature owing to intramolecular spin-exchange interaction. Cryomagnetic properties have been studied to evaluate the nature of the magnetic interaction in the complexes.

The $\chi_M T$ vs T plots for the CuMn complex (**1**) are given in Figure 4. The $\chi_M T$ value at room temperature is 3.75 K cm^3 mol^{-1} (=5.48 μ_B) which decreases with decreasing temperature to the plateau value of 2.6 Kcm^3 mol^{-1} (ca. 4.6 μ_B) near 40 K. The plateau moment corresponds to the spin-only value (4.90 μ_B) for $S_T = 2$ resulting from the spin-coupling of $S_{Cu} = {}^1/_2$ and $S_{Mn} = {}^5/_2$. A slight decrease in $\chi_M T$ is seen below 5 K which may arise from an intermolecular antiferromagnetic interaction or the zero-field splitting of Mn(II). The cryomagnetic behavior of **1** can be reproduced by the magnetic susceptibility expression (1) based on the Heisenberg model including the Weiss term (Θ) for correcting secondary effects:

$$\chi_M = \{N\beta^2/k(T-\Theta)\}[28g_3^{\,2} + 10g_2^{\,2}\exp(-6J/kT)]/[7 + 5\exp(-6J/kT)] + N\alpha \quad (1)$$

In this expression N is Avogadro's number, β is the Bohr magneton, k is the Boltzmann constant, J is the exchange integral, T is the absolute temperature, $N\alpha$ is the temperature-independent paramagnetism, and g_2 and g_3 are the g factors associated with the total spin-states $S_T = 2$ and 3, respectively. The g factors are given using local g values as follows: $g_2 = (7g_{Mn} - g_{Cu})/6$ and $g_3 = (5g_{Mn} + g_{Cu})/6$.[1,28,29] The magnetic simulation is given by the solid curve (a) in Figure 4. The best-fit parameters are $J = -32.0$ cm^{-1}, $g_{Cu} = 2.10$, $g_{Mn} = 1.95$, $N\alpha = 60 \times 10^{-6}$ cm^3 mol^{-1}, and $\Theta = -1.2$ K. The discrepancy factor defined as $R(\chi) = [\Sigma(\chi_{obs} - \chi_{cal})^2/\Sigma(\chi_{obs})^2]^{1/2}$ is 9.6×10^{-3}.

The $\chi_M T$ vs T plots for the CuCo complex (**2**) are also given in Figure 4. The $\chi_M T$ value at room temperature is 2.10 K cm^3 mol^{-1} (=4.10 μ_B) which decreases with decreasing temperature to 0.24 K cm^3 mol^{-1} (=1.40 μ_B) at liquid-helium temperature. The $\chi_M T$ value at liquid-helium temperature is smaller than the value for $S_T = 1$ resulting from the spin-coupling of $S_{Cu} = {}^1/_2$ and $S_{Co} = {}^3/_2$. This fact indicates the operation of secondary magnetic contribution such as orbital effect and/or zero-field splitting of Co(II).

Magnetic simulations were carried out on the basis of the magnetic susceptibility expression (2), where $g_1 = (5g_{Co} - g_{Cu})/4$ and $g_2 = (3g_{Co} + g_{Cu})/4$ are g factors associated with the total spin-states $S_T = 1$ and 2, respectively. A tolerable fitting was obtained as indicated by the solid curve (b) in Figure 4 using $J = -44.0$ cm^{-1}, $g_{Cu} = 2.10$, $g_{Co} = 2.25$, $N\alpha = 300 \times 10^{-6}$ cm^3 mol^{-1}, and $\Theta = -16.5$ K. Because of the significant contribution of the secondary effect, the discrepancy factor $R(\chi)$ in this simulation is large (3.8×10^{-2}).

$$\chi_M = \{N\beta^2/k(T-\Theta)\}[10g_2^{\,2} + 2g_1^{\,2}\exp(-4J/kT)]/[5 + 3\exp(-4J/kT)] + N\alpha \quad (2)$$

The $\chi_M T$ vs T plots for the CuNi complex (**3**) are given in Figure 5. The $\chi_M T$ value decreases from 0.97 K cm^3 mol^{-1} (=2.78 μ_B) at room temperature to a plateau value of 0.4 K cm^3 mol^{-1} (ca. 1.8 μ_B) near 50 K. The plateau magnetic moment corresponds to the spin-only value for $S_T = {}^1/_2$ (1.73 μ_B) resulting from the spin-coupling between $S_{Cu} = {}^1/_2$ and $S_{Ni} = 1$. Magnetic analyses have been made on the basis of magnetic susceptibility expression (3). In this expression $g_{1/2} = (4g_{Ni} - g_{Cu})/3$ and $g_{3/2} = (2g_{Ni} + g_{Cu})/3$ are g factors associated with the total spin-states $S_T = {}^1/_2$ and ${}^3/_2$, respectively.

$$\chi_M = \{N\beta^2/4k(T-\Theta)\}[10g_{3/2}^{\,2} + g_{1/2}^{\,2}\exp(-3J/kT)]/[2 + \exp(-3J/kT)] + N\alpha \quad (3)$$

(28) Chao, C. C. *J. Magn. Reson.* **1973**, *10*, 1.
(29) Scaringe, R. P.; Hodgson, D. J.; Hatfield, W. E. *Mol. Phys.* **1978**, *35*, 701.

A fairly good magnetic simulation is obtained on the basis of eq 3 using $J = -97.0$ cm^{-1}, $g_{Cu} = 2.08$, $g_{Ni} = 2.12$, $N\alpha = 220 \times 10^{-6}$ cm^{3}mol^{-1}, and $\Theta = -0.8$ K (see trace a). The discrepancy factor $R(\chi)$ in this simulation is 1.7×10^{-2}.

The cryomagnetic behavior of the CuCu complex (**5**) is given by the χ_A vs T plots in Figure 5, where χ_A means the magnetic susceptibility per one copper. The χ_A value at room temperature is 269×10^{-6} cm^3 mol^{-1} (0.79 μ_B) that decreases with decreasing temperature and reaches a plateau value of 120×10^{-6} cm^3 mol^{-1} near 140 K. The plateau value is close to but slightly larger than the temperature-independent paramagnetism for Cu(II), implying the contamination of a small amount of monomeric Cu(II) species. Thus, magnetic analyses were made on the basis of the Bleaney−Bowers equation[30] including the correction term for a paramagnetic impurity (eq 4), where ρ is

$$\chi_A = (Ng^2\beta^2/kT)[3 + \exp(-2J/kT)]^{-1}(1 - \rho) + 0.45\rho/T + N\alpha \quad (4)$$

the fraction of paramagnetic impurity. A good magnetic simulation has been obtained using the best-fit parameters $g = 2.10$, $J = -330$ cm^{-1}, $N\alpha = 60 \times 10^{-6}$ cm^3 mol^{-1}, and $\rho = 0.015$ ($R(\chi) = 9.9 \times 10^{-3}$) (trace b).

The above cryomagnetic analyses demonstrate fairly strong antiferromagnetic interaction within each core.

Spin-Doublet ESR of the CuNi Complex (3). Cryomagnetic studies indicates that the two metal ions in the CuNi complex (**3**) are perfectly spin-coupled near liquid-nitrogen temperature allowing thermal population only on the spin-doublet ground state. For the Ni(II) in this complex a pseudooctahedral geometry with two unidentate perchlorate ions at the apical sites is predicted from the IR spectrum. A similar six-coordination about the Ni(II) may be preserved in dmf solution where the axial sites are occupied by solvent dmf molecules. The EPR spectrum of **3** (frozen DMF solution at liquid-nitrogen temperature) is of an axial pattern with $g_{||} = 2.09$ and $g_\perp = 2.24$ and on the $g_{||}$ component is superposed a four-line hyperfine structure due to the Cu nucleus ($A_{//} = 58 \times 10^{-4}$ cm^{-1}) (see Figure 6). A similar ESR spectrum was observed in our laboratory for a related macrocyclic CuNi complex.[31] In Figure 6 is given the ESR spectrum of the CuZn complex (**5**) for comparison (frozen DMF solution at liquid-nitrogen temperature) that has the parameters $g_{||} = 2.21$, $g_\perp = 2.05$, and $A_{||} = 172 \times 10^{-4}$ cm^{-1}. It must be noted that **3** and **5** differ from each other with respect to the relative locations of $g_{||}$ and $g_\perp$. The relation $g_{||} > g_\perp$ of **5** is typical of axially symmetric Cu(II) having one unpaired electron in a $d_{x^2-y^2}$ orbital whereas the relation $g_{||} < g_\perp$ is seen for Cu(II) having one unpaired electron in a d_{z^2} orbital.[32]

The EPR hyperfine coupling constants A'_a and A'_b of a magnetically coupled M_a-M_b system are given by the local hyperfine coupling constants A_a and A_b as follows:[28,29,33]

$$A'_a = (1 + C)A_a/2$$

$$A'_b = (1 - C)A_b/2$$

$$C = [S_a(S_a + 1) - S_b(S_b + 1)]/S(S + 1)$$

In these equations S_a and S_b denote the spins of M_a and M_b, respectively, and S denotes the total spin in the coupled M_a-M_b. The hyperfine structure in spin-coupled $Cu^{II}Ni^{II}$ is simple because only Cu has isotopes ^{63}Cu (69.1%) and ^{65}Cu (30.9%) with $I_{Cu} = {}^3/_2$. Ni has isotope ^{61}Ni with $I_{Ni} = {}^3/_2$, but its natural abundance is very low (1.25%). Thus, only the hyperfine structure due to the Cu nucleus is observed for spin-coupled $Cu^{II}Ni^{II}$. For the spin-doublet state of the Cu(II)($S_{Cu} = {}^1/_2$)−Ni(II)($S_{Ni} = 1$) system, the constant C is calculated to be $-{}^5/_3$ using $S_{Cu} = {}^1/_2$, $S_{Ni} = 1$, and $S = {}^1/_2$ and the hyperfine coupling constant A'_{Cu} is expressed by the correlation $A'_{Cu} = -A_{Cu}/3$. If we adopt the hyperfine coupling constant of the CuZn complex **5** ($A_{Cu} = 172 \times 10^{-4}$ cm^{-1}) as the local copper hyperfine constant for **3**, the observed A'_{Cu} (58×10^{-4} cm^{-1}) is indeed one-third of that of **5**.

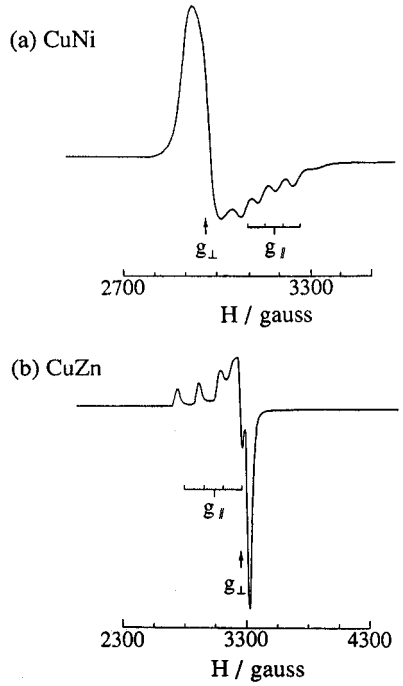

Figure 6. X-band ESR spectra of (a) CuNi complex **3** and (b) CuZn complex **5**.

The exchange integral J between Cu(II) and Ni(II) is given by means of two individual exchanges: $J = {}^1/_2\{J[d_{x^2-y^2}(Cu),d_{x^2-y^2}(Ni)] + J[d_{x^2-y^2}(Cu),d_{z^2}(Ni)]\}$. The first term must be largely negative as proved for dinuclear Cu(II) complexes;[34,35] the second term is believed to be weakly antiferromagnetic.[35] As a result of the spin coupling through the $d_{x^2-y^2}(Cu)-p(O)-d_{x^2-y^2}(Ni)$ pathway there remains one unpaired electron on the $d_{z^2}(Ni)$ orbital. The EPR spectrum exhibiting the Cu hyperfine structure, however, clearly indicates that the unpaired electron resides on the molecular orbital of d_{z^2} character comprising $d_{z^2}(Cu)$ and $d_{z^2}(Ni)$ and is delocalized over the CuNi core.

Acknowledgment. This work was supported by a Grant-in-Aid for Scientific Research (No. 07454178) from the Ministry of Education, Science, and Culture of Japan. Thanks are also due to The Daiwa Anglo-Japanese Foundation and The British Council for support.

Supporting Information Available: Analytical results for all the compounds and listings of atomic positional and thermal parameters, anisotropic thermal parameters, and full bond distances and bond angles (27 pages). X-ray crystallographic files, in CIF format, are available. Access and ordering information is given on any current masthead page.

IC9614430

(30) Bleaney, B.; Bowers, K. D. *Proc. R. Soc. London, Ser. A* **1952**, *214*, 451.
(31) Aono, T.; Wada, H.; Aratake, Y.; Matsumoto, N.; Ōkawa, H.; Matsuda, Y. *J. Chem. Soc., Dalton Trans.* **1996**, 25.
(32) Goodman, B. A.; Raynor, J. B. *Adv. Inorg. Chem. Radiochem.* **1970**, *13*, 135.
(33) Buluggiu, E. *J. Phys. Chem. Solid.* **1980**, *41*, 1175.
(34) Melnik, M. *Coord. Chem. Rev.* **1982**, *42*, 259.
(35) Cairns, C. J.; Busch, D. H. *Coord. Chem. Rev.* **1986**, *69*, 1.